Orbital stabilization of a VToL UAV for landing on oscillating platforms

Vincenzo Lippiello and Fabio Ruggiero

Abstract— **This paper presents preliminary theoretical results about asymptotic orbital stabilization of an aerial vehicle for landing on a periodic oscillating platform. A feedback controller firstly stabilizes a chosen set of virtual geometric constraints. This pushes the dynamics of the aerial vehicle to reach a limit cycle, that is in turn the periodic motion of the landing platform to track. Then, a linear periodic system is considered around the vicinity of the orbit, and it is stabilized through a modified LQR design. Mathematical and theoretical frameworks are presented along with case studies that are critically discussed.**

I. Introduction

Due to their versatility and astounding skills, vertical take-off-and-landing (VToL) unmanned aerial vehicles (UAVs) are beginning to be employed in uncertain environments and hazardous situations. They are then migrating from passive tasks like inspection, surveillance and monitoring, to active tasks like grasping and manipulation. Operating in uncertain environments is a great challenge due to unexpected situations, specially in outdoor scenarios. Therefore, UAVs have recently been equipped with a robotic arm to enhance their manipulation capabilities [1]. In addition, some works estimate the external disturbances and the unmodeled effects [2], [3].

A challenging problem in autonomous flight is the design of controllers for landing in uncertain conditions. For instance, a safe landing in case of failure of one propeller is addressed in [4], [5]. The problem of safe landing on oscillating platforms is of significant interest as well, and this manuscript deals with such a situation.

In the literature, several works cope with the problem of autonomous landing of an aerial vehicle on an oscillating platform (e.g., a ship's deck, a moving rover, a sliding track, etc.), which is useful in various tasks and scenarios like search and rescue, robot collaboration and synchronization, field robotics, and so on. Three main approaches can be recognized within the related state of the art.

The former approach relies on an a-priori knowledge of the oscillating trajectory obtained through a predictive model of the landing platform. In case the prediction/estimation is accurate, the resulting performance of the landing manoeuvre is precise as well. As a drawback, it might be sometimes difficult to determine a reliable model and an estimate of the oscillating motion. A Fourier transform-based method is employed in [6] to characterize the motion of the sea and the ship dynamics. Afterwards, a landing control algorithm is developed on the basis of the relative dynamics between the UAV and the ship. A complete ship's deck simulation for autonomous landing of a VToL UAV is proposed in [7]. The pose of the landing platform is then measured using a single downward looking camera. A Kalman filter uses such measures to calculate the state of the ship's deck, which is in turn employed to solve the autonomous landing problem. A vision system to detect and track international landing makers, and measure the relative pose between the aerial vehicle and a ship's deck, is instead employed in [8].

The second approach relies on a real-time tracking of the oscillating reference. This method is useful in case the oscillating motion is an unknown function of time. Feedback control is then exploited to overcome this issue. The design of an internal model-based autopilot is introduced in [9]. The vertical motion of a deck is a superposition of a fixed number of sinusoidal functions of time with unknown frequency, amplitude and phase. The zero-error manifold is shown to be globally stable. The method in [10] is instead split in two phases: the aerial vehicle is first stabilized with respect to the moving platform at a constant offset through a nonlinear PI-based controller; after, the automatic vertical landing is regulated thanks to vertical optical flow measurements. Lyapunov analysis is used to prove global stability and convergence to the desired goal.

The latter approach is a combination of the first two. As underlined in [11], there is no guarantee that only feedback control can fulfil the landing task. Input saturation and physical limitations of the aerial vehicle may constraint the controller performance. On the other hand, a feedback controller can benefit from some feedforward information related to the oscillating platform. An estimation module is then required as for the first approach described above. The relative distance between the UAV and the platform is employed in [11] to estimate the oscillating motion. An Uscented Kalman Filter is employed to estimate the requested parameters that are fed back in turn to both a trajectory generation module and an adaptive tracking controller.

From the above analysis, it is possible to notice how there are no works directly considering the stabilization of a VToL UAV on the oscillating trajectory of the landing platform. Once that such a motion is available/estimated, most of the manuscripts consider a motion planner or use such information in feedforward. In this paper, a preliminary

Authors are listed in alphabetical order. The research leading to these results has been supported by the SHERPA and AEROARMS large-scale integrating projects, funded by the European Community under grants FP7-ICT-600958 and H2020-ICT-644271, respectively.The authors are solely responsible for its content.

Authors are with the PRISMA Lab, CREATE Consortium and Department of Electrical Engineering and Information Technology, University of Naples Federico II, via Claudio 21, 80125, Naples, Italy. Corresponding author's email fabio.ruggiero@unina.it.

work for asymptotic orbital stabilization is instead proposed. The method is mainly based on the work in [12], in which a constructive tool for orbital stabilization of mechanical systems with degree of underactuation one is introduced. This method has also been employed in nonprehensile manipulation tasks [13], and to control the attitude of a UAV [14], [15], but without considering the position of the aerial vehicle as instead done in this paper. Given the dynamic model of a UAV, a set of virtual geometric constraints is imposed. It is possible to check that once these constraints are reached through a feedback control, this forces the system to exhibit a limit cycle (i.e., a periodic trajectory). Keeping the system on this periodic trajectory satisfies the desired task. Notice that most of VToL UAVs have two degrees of underactuation, therefore one translational component of the aerial vehicle is here neglected to fit the assumptions in [12]. Furthermore, a generic sinusoidal function with a given amplitude, frequency and phase is the considered oscillating trajectory: how these parameters are determined is out the scope of this manuscript. The introduced novelty is mainly a new application for the considered orbital stabilization tool: as further explained at the end of the manuscript, this paper is the necessary first step towards more sophisticated controllers.

The outline of the paper is as follows. In order to make the paper self-contained, Sections II and III recap the orbital stabilization approach proposed in [12] and the derivation of the dynamic model for a VToL UAV, respectively. Afterwards, the orbital stabilization approach specified for the considered aerial task is developed in Section IV. Case studies are presented and critically discussed in V. Section VI concludes the manuscript with a discussion about possible further developments.

II. Mathematical background

This section offers a brief mathematical recap of the constructive tool for orbital stabilization presented in [12]. Interested readers may look at the cited work and references therein for more details and the proofs.

Consider the dynamic model of a controlled Lagrangian system in the following form

$$\boldsymbol{B}(\boldsymbol{q})\ddot{\boldsymbol{q}} + \boldsymbol{C}(\boldsymbol{q},\dot{\boldsymbol{q}})\dot{\boldsymbol{q}} + \boldsymbol{g}(\boldsymbol{q}) = \boldsymbol{G}(\boldsymbol{q})\boldsymbol{\tau}, \tag{1}$$

where $\boldsymbol{q} = \begin{bmatrix} q_1 & \dots & q_n \end{bmatrix}^{\mathrm{T}} \in \mathbb{R}^n$ and $\dot{\boldsymbol{q}} \in \mathbb{R}^n$ are the general coordinates and the related time derivative vectors, respectively; $\boldsymbol{B}(\boldsymbol{q}) \in \mathbb{R}^{n\times n}$ is the symmetric positive definite inertia matrix; $\boldsymbol{C}(\boldsymbol{q},\dot{\boldsymbol{q}}) \in \mathbb{R}^{n\times n}$ is the Coriolis matrix; $\boldsymbol{g}(\boldsymbol{q}) \in \mathbb{R}^n$ is the gravity vector; $\boldsymbol{\tau} \in \mathbb{R}^m$ is the independent control input vector and $\boldsymbol{G}(\boldsymbol{q}) \in \mathbb{R}^{n\times m}$ is a proper selection matrix. In this paper, the considered mechanical system (1) is underactuated with degree of underactuation $n - m = 1$.

It is possible to show that if feedback stabilization of a chosen set of $n-1$ independent geometric relations (called *virtual holonomic constraints*)

$$q_1 = \phi_1(\lambda,\boldsymbol{c}), \quad \dots \quad q_n = \phi_n(\lambda,\boldsymbol{c}), \tag{2}$$

is achievable, then the zero dynamics (often called *virtual limit system*) of the mechanical system (1) can be written as

$$\alpha(\lambda,\boldsymbol{c})\ddot{\lambda} + \beta(\lambda,\boldsymbol{c})\dot{\lambda}^2 + \gamma(\lambda,\boldsymbol{c}) = 0, \tag{3}$$

where $\lambda \in \mathbb{R}$ is a new independent scalar; $\boldsymbol{c}$ is a vector of constant parameters useful to define the n relationships in (2). By defining $\boldsymbol{\iota}(\boldsymbol{q}) \in \mathbb{R}^n$ as the vector such that $\boldsymbol{\iota}(\boldsymbol{q})^{\mathrm{T}}\boldsymbol{G}(\boldsymbol{q})\boldsymbol{\tau} = 0$, $\forall \boldsymbol{q}$, and

$$\boldsymbol{\phi}(\lambda,\boldsymbol{c}) = \begin{bmatrix}\phi_1(\lambda,\boldsymbol{c}) & \dots & \phi_n(\lambda,\boldsymbol{c})\end{bmatrix}^{\mathrm{T}} \in \mathbb{R}^n, \tag{4a}$$

$$\boldsymbol{\phi}'(\lambda,\boldsymbol{c}) = \begin{bmatrix}\phi_1'(\lambda,\boldsymbol{c}) & \dots & \phi_n'(\lambda,\boldsymbol{c})\end{bmatrix}^{\mathrm{T}} \in \mathbb{R}^n, \tag{4b}$$

$$\boldsymbol{\phi}''(\lambda,\boldsymbol{c}) = \begin{bmatrix}\phi_1''(\lambda,\boldsymbol{c}) & \dots & \phi_n''(\lambda,\boldsymbol{c})\end{bmatrix}^{\mathrm{T}} \in \mathbb{R}^n, \tag{4c}$$

where $'$ denotes the derivative with respect to λ, it is then possible to express the scalar terms in (3) as

$$\alpha(\lambda) = \boldsymbol{\iota}(\boldsymbol{q})^{\mathrm{T}}\boldsymbol{B}(\boldsymbol{q})\boldsymbol{\phi}'(\lambda)|_{\boldsymbol{q}=\boldsymbol{\phi}(\lambda)}, \tag{5a}$$

$$\beta(\lambda) = \boldsymbol{\iota}(\boldsymbol{q})^{\mathrm{T}}\left(\boldsymbol{C}(\boldsymbol{q},\dot{\boldsymbol{q}})\boldsymbol{\phi}'(\lambda) + \boldsymbol{B}(\boldsymbol{q})\boldsymbol{\phi}''(\lambda)\right)|_{\boldsymbol{q}=\boldsymbol{\phi}(\lambda)}, \tag{5b}$$

$$\gamma(\lambda) = \boldsymbol{\iota}(\boldsymbol{q})^{\mathrm{T}}\boldsymbol{g}(\boldsymbol{q})|_{\boldsymbol{q}=\boldsymbol{\phi}(\lambda)}, \tag{5c}$$

in which the dependence on $\boldsymbol{c}$ is neglected from now on to simplify the notation. If it is possible to find a feedback controller $\boldsymbol{\tau} = \boldsymbol{\tau}^\star$ rendering the virtual geometric constraints (2) asymptotically invariant, then λ satisfies (3). Moreover, supposing that $\alpha(\lambda)$ has only isolated zeros, if the solution $(\lambda(t),\dot{\lambda}(t))$ of (3) exists with initial conditions $\lambda(0) = \lambda_0$, $\dot{\lambda}(0) = \dot{\lambda}_0$ and it is continuously differentiable, then the following integral of motion

$$I(\lambda,\dot{\lambda},\lambda_0,\dot{\lambda}_0) = \dot{\lambda}^2 - \psi(\lambda_0,\lambda)\left(\dot{\lambda}_0^2 - 2\int_{\lambda_0}^{\lambda}\psi(s,\lambda_0)\frac{\gamma(s)}{\alpha(s)}\mathrm{d}s\right) \tag{6}$$

preserves its zero value along the solution $(\lambda(t),\dot{\lambda}(t))$, with

$$\psi(\lambda_a,\lambda_b) = \exp\left(-2\int_{\lambda_a}^{\lambda_b}\frac{\beta(s)}{\alpha(s)}\mathrm{d}s\right). \tag{7}$$

Notice that, in general, not each virtual constraint in (2) is stabilizable. A virtual holonomic constraint is said to be *regular* if $\alpha(\lambda) \neq 0, \forall \boldsymbol{q} \in \mathbb{R}^n$ [16]. This condition is similar to the one required to define the integral of motion (6), and under mild conditions allows the virtual holonomic constraints to be stabilizable [16].

Therefore, given a set of regular virtual constraints (2), suppose that exists a vector $\boldsymbol{c}$ such that the resulting virtual limit system (3) has a T-periodic solution

$$\lambda^\star(t) = \lambda^\star(t+T), \tag{8}$$

for each time t. The problem is then the design of a feedback controller $\boldsymbol{\tau} = \boldsymbol{\tau}^\star$ that guarantees the invariance of (2) and the orbital asymptotic stability of (8).

Consider now the following new coordinates

$$y_1 = q_1 - \phi_1(\lambda), \quad \dots \quad y_n = q_n - \phi_n(\lambda). \tag{9}$$

One of these coordinates can be always locally expressed as function of the others. Without loss of generality, let y_n be expressed as function of λ and y_i, with $i = 1, \dots, n-1 = m$. Therefore, it is possible to express the last equation of (9) as follows

$$q_n = \phi_n(\lambda) + h(y_1, \dots, y_m, \lambda), \tag{10}$$

with h a scalar smooth function of its arguments. Consider the vectors $\boldsymbol{y} = \begin{bmatrix} y_1 & \dots & y_m \end{bmatrix}^{\mathrm{T}} \in \mathbb{R}^m$ and $\boldsymbol{\varsigma} = \begin{bmatrix} \boldsymbol{y}^{\mathrm{T}} & \lambda \end{bmatrix}^{\mathrm{T}} \in \mathbb{R}^n$. Taking the first and second time derivatives of (9) yields

$$\dot{\boldsymbol{q}} = \boldsymbol{L}(\boldsymbol{\varsigma})\dot{\boldsymbol{\varsigma}}, \tag{11a}$$

$$\ddot{\boldsymbol{q}} = \boldsymbol{L}(\boldsymbol{\varsigma})\ddot{\boldsymbol{\varsigma}} + \boldsymbol{n}(\boldsymbol{\varsigma}, \dot{\boldsymbol{\varsigma}}), \tag{11b}$$

with

$$\boldsymbol{L}(\boldsymbol{\varsigma}) = \begin{bmatrix} \boldsymbol{I}_m & \boldsymbol{0}_m \\ \frac{\partial h}{\partial \boldsymbol{\varsigma}} & \end{bmatrix} \in \mathbb{R}^{n \times n}, \tag{12a}$$

$$\boldsymbol{n}(\boldsymbol{\varsigma}, \dot{\boldsymbol{\varsigma}}) = \dot{\boldsymbol{L}}(\boldsymbol{\varsigma})\dot{\boldsymbol{\varsigma}} \in \mathbb{R}^n, \tag{12b}$$

where $\boldsymbol{I}_a \in \mathbb{R}^{a \times a}$ and $\boldsymbol{0}_a \in \mathbb{R}^a$ are the identity matrix and the zero vector, respectively. Notice that in case the virtual holonomic constraints (2) are invariant, then $\boldsymbol{y} \to \boldsymbol{0}_m$ asymptotically.

Consider now the following terms

$$\boldsymbol{K}(\boldsymbol{\varsigma}) = \boldsymbol{E}\boldsymbol{L}(\boldsymbol{\varsigma})^{-1}\boldsymbol{B}(\boldsymbol{q})^{-1}\boldsymbol{G}(\boldsymbol{q}) \in \mathbb{R}^{m \times m}, \tag{13a}$$

$$\boldsymbol{w}(\boldsymbol{\varsigma}, \dot{\boldsymbol{\varsigma}}) = -\boldsymbol{E}\boldsymbol{L}(\boldsymbol{\varsigma})^{-1}\boldsymbol{B}(\boldsymbol{q})^{-1}\left(\boldsymbol{C}(\boldsymbol{q}, \dot{\boldsymbol{q}})\dot{\boldsymbol{q}} + \boldsymbol{g}(\boldsymbol{q})\right) \in \mathbb{R}^m, \tag{13b}$$

with $\boldsymbol{E} = \begin{bmatrix} \boldsymbol{I}_m & \boldsymbol{0}_m \end{bmatrix} \in \mathbb{R}^{m \times n}$, $q_1 = y_1 + \phi_1(\lambda)$, $\dots, q_{n-1} = y_{n-1} + \phi_{n-1}(\lambda)$, $q_n = \phi_n(\lambda) + h(\boldsymbol{\varsigma})$, and the hypothesis that both $\boldsymbol{L}(\boldsymbol{\varsigma})$ and $\boldsymbol{K}(\boldsymbol{\varsigma})$ are nonsingular in a neighbourhood of the desired orbit (8). The feedback transformation

$$\boldsymbol{\tau} = \boldsymbol{K}(\boldsymbol{\varsigma})^{-1}\left(\boldsymbol{\upsilon} - \boldsymbol{w}(\boldsymbol{\varsigma}, \dot{\boldsymbol{\varsigma}})\right), \tag{14}$$

with $\boldsymbol{\upsilon} \in \mathbb{R}^m$ a new virtual input, brings the closed-loop dynamics of (1) into the following partially-linear form

$$\begin{aligned} \alpha(\lambda)\ddot{\lambda} + \beta(\lambda)\dot{\lambda}^2 + \gamma(\lambda) = {} & \boldsymbol{g}_y(\boldsymbol{\varsigma}, \dot{\boldsymbol{\varsigma}}, \ddot{\lambda})^{\mathrm{T}}\boldsymbol{y} \\ & + \boldsymbol{g}_{\dot{y}}(\boldsymbol{\varsigma}, \dot{\boldsymbol{\varsigma}}, \ddot{\lambda})^{\mathrm{T}}\dot{\boldsymbol{y}} \\ & + \boldsymbol{g}_{\upsilon}(\boldsymbol{\varsigma}, \dot{\boldsymbol{\varsigma}})^{\mathrm{T}}\boldsymbol{\upsilon}, \end{aligned} \tag{15a}$$

$$\ddot{\boldsymbol{y}} = \boldsymbol{\upsilon}. \tag{15b}$$

Notice that the left-hand side of (15a) is the virtual limit system (3), while the right-hand side presents smooth functions whose expressions are given in Appendix A.

The objective is now to bring $\boldsymbol{y}$ to zero through $\boldsymbol{\upsilon}$. Let $\boldsymbol{g}_y^\star(t)$, $\boldsymbol{g}_{\dot{y}}^\star(t)$ and $\boldsymbol{g}_{\upsilon}^\star(t)$ be the functions $\boldsymbol{g}_y(\boldsymbol{\varsigma}, \dot{\boldsymbol{\varsigma}}, \ddot{\lambda})$, $\boldsymbol{g}_{\dot{y}}(\boldsymbol{\varsigma}, \dot{\boldsymbol{\varsigma}}, \ddot{\lambda})$ and $\boldsymbol{g}_{\upsilon}(\boldsymbol{\varsigma}, \dot{\boldsymbol{\varsigma}})$, respectively, evaluated at $\lambda(t) = \lambda^\star(t)$ and $\boldsymbol{y} = \boldsymbol{0}_m$. It is possible to consider the following auxiliary linear system

$$\begin{aligned} \dot{I} = 2\frac{\dot{\lambda}^\star(t)}{\alpha(\lambda^\star(t))}\big(& \boldsymbol{g}_y^\star(t)^{\mathrm{T}}\boldsymbol{y} + \boldsymbol{g}_{\dot{y}}^\star(t)^{\mathrm{T}}\dot{\boldsymbol{y}} + \boldsymbol{g}_{\upsilon}^\star(t)^{\mathrm{T}}\boldsymbol{\upsilon} \\ & - \beta(\lambda^\star(t))I\big), \end{aligned} \tag{16a}$$

$$\ddot{\boldsymbol{y}} = \boldsymbol{\upsilon}, \tag{16b}$$

with $\dot{I}$ the time derivative of (6). The state-space representation of (16) is given by

$$\dot{\boldsymbol{\zeta}} = \boldsymbol{A}(t)\boldsymbol{\zeta} + \boldsymbol{V}(t)^{\mathrm{T}}\boldsymbol{\upsilon}, \tag{17}$$

with $\boldsymbol{\zeta} = \begin{bmatrix} I(\lambda, \dot{\lambda}, \lambda^\star(0), \dot{\lambda}^\star(0)) & \boldsymbol{y}^{\mathrm{T}} & \dot{\boldsymbol{y}}^{\mathrm{T}} \end{bmatrix}^{\mathrm{T}} \in \mathbb{R}^{2m+1}$ and

$$\boldsymbol{A}(t) = \begin{bmatrix} \kappa_1(t) & \boldsymbol{\kappa}_2(t)^{\mathrm{T}} & \boldsymbol{\kappa}_3(t)^{\mathrm{T}} \\ \boldsymbol{0}_m & \boldsymbol{O}_m & \boldsymbol{I}_m \\ \boldsymbol{0}_m & \boldsymbol{O}_m & \boldsymbol{O}_m \end{bmatrix} \in \mathbb{R}^{2m+1 \times 2m+1}, \tag{18a}$$

$$\boldsymbol{V}(t) = \begin{bmatrix} \boldsymbol{\rho}(t) & \boldsymbol{O}_m & \boldsymbol{I}_m \end{bmatrix} \in \mathbb{R}^{m \times 2m+1}, \tag{18b}$$

where

$$\kappa_1(t) = -2\dot{\lambda}^\star(t)\frac{\beta(\lambda^\star(t))}{\alpha(\lambda^\star(t))} \in \mathbb{R}, \tag{19a}$$

$$\boldsymbol{\kappa}_2(t) = 2\dot{\lambda}^\star(t)\frac{\boldsymbol{g}_y^\star(t)}{\alpha(\lambda^\star(t))} \in \mathbb{R}^m, \tag{19b}$$

$$\boldsymbol{\kappa}_3(t) = 2\dot{\lambda}^\star(t)\frac{\boldsymbol{g}_{\dot{y}}^\star(t)}{\alpha(\lambda^\star(t))} \in \mathbb{R}^m, \tag{19c}$$

$$\boldsymbol{\rho}(t) = 2\dot{\lambda}^\star(t)\frac{\boldsymbol{g}_{\upsilon}^\star(t)}{\alpha(\lambda^\star(t))} \in \mathbb{R}^m, \tag{19d}$$

and $\boldsymbol{O}_a \in \mathbb{R}^{a \times a}$ is a zero matrix of proper dimensions. Notice that $\boldsymbol{A}(t) = \boldsymbol{A}(t+T)$ and $\boldsymbol{V}(t) = \boldsymbol{V}(t+T)$, meaning that (17) is a linear periodic system. In case (17) is controllable, then the following input

$$\boldsymbol{\upsilon} = -\boldsymbol{\Gamma}^{-1}\boldsymbol{V}(t)\boldsymbol{R}(t)\boldsymbol{\zeta}, \tag{20}$$

exponentially stabilizes (16). This means that both I and $\boldsymbol{y}$ with their time derivatives go to zero as desired. The periodic matrix $\boldsymbol{R}(t) = \boldsymbol{R}(t+T) \in \mathbb{R}^{2m+1 \times 2m+1}$ is the solution of the periodic Riccati equation

$$\begin{aligned} \dot{\boldsymbol{R}}(t) + \boldsymbol{A}(t)^{\mathrm{T}}\boldsymbol{R}(t) + \boldsymbol{R}(t)\boldsymbol{A}(t) + \boldsymbol{\Theta} \\ = \boldsymbol{R}(t)\boldsymbol{V}(t)^{\mathrm{T}}\boldsymbol{\Gamma}^{-1}\boldsymbol{V}(t)\boldsymbol{R}(t), \end{aligned} \tag{21}$$

with $\boldsymbol{\Gamma} \in \mathbb{R}^{m \times m}$ and $\boldsymbol{\Theta} \in \mathbb{R}^{2m+1 \times 2m+1}$ symmetric and positive definite gain matrices.

Nevertheless, notice that (20) stabilizes (16), but not (15), which is instead what desired. The following ad-hoc modification is thus proposed in [12]

$$\boldsymbol{\upsilon} = -\boldsymbol{\Gamma}^{-1}\bar{\boldsymbol{V}}(t)\boldsymbol{R}(t)\boldsymbol{\zeta}, \tag{22}$$

with $\bar{\boldsymbol{V}}(t)$ equals to $\boldsymbol{V}(t)$ but with the following change to (19d)

$$\bar{\boldsymbol{\rho}}(t) = 2\dot{\lambda}(t)\frac{\boldsymbol{g}_{\upsilon}(\boldsymbol{\varsigma}, \dot{\boldsymbol{\varsigma}})}{\alpha(\lambda(t))}. \tag{23}$$

Therefore, the control laws (22) and (14) stabilize the virtual holonomic constraints (2) and lead the closed-loop system to the periodic orbital trajectory (8), that is the solution of the virtual limit system (3).

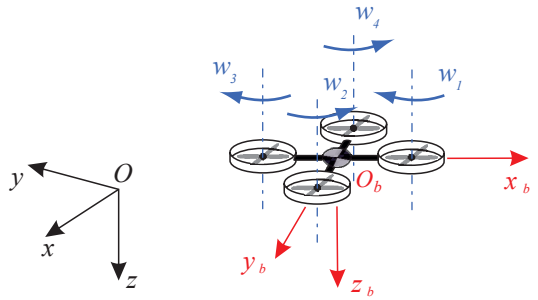

Fig. 1. A VToL UAV and the related reference frames. The inertial frame Σ_i is depicted in black. The body frame Σ_b is in red. The motor propellers speed and the related labels are depicted in blue.

III. Dynamic model of a VToL UAV

Looking at Fig. 1, consider a world-fixed inertial frame Σ_i and a body-fixed reference frame Σ_b attached to the center of mass (c.o.m.) of the VToL UAV. The attitude of the aerial vehicle is given by the rotation matrix $\boldsymbol{R}_b \in SO(3)$. Using the roll-pitch-yaw Euler angles, $\boldsymbol{\eta}_b = \begin{bmatrix}\phi & \theta & \Psi\end{bmatrix}^{\mathrm{T}}$, the rotation matrix is expressed as follows

$$\boldsymbol{R}_b(\boldsymbol{\eta}_b) = \begin{bmatrix} c_\theta c_\Psi & s_\phi s_\theta c_\Psi - c_\phi s_\Psi & c_\phi s_\theta c_\Psi + s_\phi s_\Psi \\ c_\theta s_\Psi & s_\phi s_\theta s_\Psi + c_\phi c_\Psi & c_\phi s_\theta s_\Psi - s_\phi c_\Psi \\ -s_\theta & s_\phi c_\theta & c_\phi c_\theta \end{bmatrix}, \tag{24}$$

where sine and cosine are abbreviated with $s_\times$ and $c_\times$, respectively. The position of the UAV's c.o.m., that is the origin of Σ_b with respect to Σ_i, is denoted by $\boldsymbol{p}_b = \begin{bmatrix}x & y & z\end{bmatrix}^{\mathrm{T}} \in \mathbb{R}^3$. On the other hand, the angular velocity of Σ_b with respect to Σ_i is denoted by $\boldsymbol{\omega}_b \in \mathbb{R}^3$. The body angular velocity of the UAV is instead given by $\boldsymbol{\omega}_b^b = \boldsymbol{R}(\boldsymbol{\eta}_b)^{\mathrm{T}}\boldsymbol{\omega}_b \in \mathbb{R}^3$. The relation between $\boldsymbol{\omega}_b^b$ and the time derivative of the Euler angles is

$$\boldsymbol{\omega}_b^b = \boldsymbol{Q}(\boldsymbol{\eta}_b)\dot{\boldsymbol{\eta}}_b, \tag{25}$$

with $\boldsymbol{Q}(\boldsymbol{\eta}_b) \in \mathbb{R}^{3\times3}$ a proper transformation matrix [3] with a singularity at $\theta = \pm\frac{\pi}{2}$, which is supposed to be far from operating conditions in this work.

The Newton-Euler formulation in [17] yields the dynamic model of a VToL UAV

$$m\ddot{\boldsymbol{p}}_b^b = -m\boldsymbol{S}(\boldsymbol{\omega}_b^b)\dot{\boldsymbol{p}}_b^b + mg\boldsymbol{R}_b(\boldsymbol{\eta}_b)^{\mathrm{T}}\boldsymbol{e}_3 + \boldsymbol{f}_b^b, \tag{26a}$$
$$\dot{\boldsymbol{R}}_b(\boldsymbol{\eta}_b) = \boldsymbol{R}(\boldsymbol{\eta}_b)\boldsymbol{S}(\boldsymbol{\omega}_b), \tag{26b}$$
$$\boldsymbol{J}_b\dot{\boldsymbol{\omega}}_b^b = -\boldsymbol{S}(\boldsymbol{\omega}_b^b)\boldsymbol{J}_b\boldsymbol{\omega}_b^b + \boldsymbol{\tau}_b^b, \tag{26c}$$

where $\ddot{\boldsymbol{p}}_b^b$ is the linear acceleration of the UAV's c.o.m. expressed in Σ_b; $\boldsymbol{e}_3 = \begin{bmatrix}0 & 0 & 1\end{bmatrix}^{\mathrm{T}} \in \mathbb{R}^3$ is a selection vector; $m > 0$ is the mass of the aerial vehicle; $\boldsymbol{J}_b \in \mathbb{R}^{3\times3}$ is the constant inertia matrix of the UAV expressed with respect to Σ_b; $\dot{\boldsymbol{\omega}}_b^b$ is the angular acceleration of the UAV expressed with respect to Σ_b; $\boldsymbol{S}(\cdot) \in \mathbb{R}^{3\times3}$ is the skew-symmetric matrix; $g = 9.81$ m/s^2 is the gravity acceleration; $\boldsymbol{f}_b^b \in \mathbb{R}^3$ and $\boldsymbol{\tau}_b^b \in \mathbb{R}^3$ are the forces and torques input vectors, respectively, expressed in Σ_b.

Usually, VToL UAVs are underactuated platforms with six degrees of freedom and four main control inputs. Among the most popular configurations of VToL UAVs there are the *quadrotor* (represented in Fig. 1) and the *hexarotors*, equipped with four and six propellers, respectively. Therefore, many UAVs have three control torques $\boldsymbol{\tau}_b^b = \begin{bmatrix}\tau_\phi & \tau_\theta & \tau_\Psi\end{bmatrix}^{\mathrm{T}}$, and one input control force $\boldsymbol{f}_b^b = \begin{bmatrix}0 & 0 & u\end{bmatrix}^{\mathrm{T}}$, with u denoting the so-called thrust, which is perpendicular to the rotation plane characterized by the propellers. A relation exists between the three control torques and the thrust with the speed velocity w_i, $i = 1, \dots, 4$ in case of a quadrotor, or $i = 1, \dots, 6$ in case of a hexarotor. This is out of the scope of this manuscript: more details can be found in [3], [17].

Considering the above introduced expression for the input force and torque, and the equations (25) and (26), it is possible to write the UAV dynamic model with respect to Σ_i as follows

$$m\ddot{\boldsymbol{p}}_b = mg\boldsymbol{e}_3 - u\boldsymbol{R}_b(\boldsymbol{\eta}_b)\boldsymbol{e}_3, \tag{27a}$$
$$\boldsymbol{M}(\boldsymbol{\eta}_b)\ddot{\boldsymbol{\eta}}_b = -\boldsymbol{D}(\boldsymbol{\eta}_b, \dot{\boldsymbol{\eta}}_b)\dot{\boldsymbol{\eta}}_b + \boldsymbol{Q}(\boldsymbol{\eta}_b)^{\mathrm{T}}\boldsymbol{\tau}_b^b, \tag{27b}$$

where $\boldsymbol{M}(\boldsymbol{\eta}_b) = \boldsymbol{Q}(\boldsymbol{\eta}_b)^{\mathrm{T}}\boldsymbol{J}_b\boldsymbol{Q}(\boldsymbol{\eta}_b) \in \mathbb{R}^{3\times3}$ is the symmetric and positive definite (considering $\theta \neq \pm\frac{\pi}{2}$) inertia matrix of the aerial vehicle related to the rotation part, and $\boldsymbol{D}(\boldsymbol{\eta}_b, \dot{\boldsymbol{\eta}}_b) = \boldsymbol{Q}(\boldsymbol{\eta}_b)^{\mathrm{T}}\boldsymbol{S}(\boldsymbol{Q}(\boldsymbol{\eta}_b)\dot{\boldsymbol{\eta}}_b)\boldsymbol{J}_b\boldsymbol{Q}(\boldsymbol{\eta}_b) + \boldsymbol{Q}(\boldsymbol{\eta}_b)^{\mathrm{T}}\boldsymbol{J}_b\dot{\boldsymbol{Q}}(\boldsymbol{\eta}_b, \dot{\boldsymbol{\eta}}_b) \in \mathbb{R}^{3\times3}$ is the Coriolis matrix for the rotation part.

Choose now $\boldsymbol{\tau}_b^b = \boldsymbol{Q}(\boldsymbol{\eta}_b)^{-\mathrm{T}}\boldsymbol{M}(\boldsymbol{\eta}_b)\bar{\boldsymbol{\tau}}_b^b + \boldsymbol{Q}(\boldsymbol{\eta}_b)^{-\mathrm{T}}\boldsymbol{D}(\boldsymbol{\eta}_b, \dot{\boldsymbol{\eta}}_b)\dot{\boldsymbol{\eta}}_b$, with $\bar{\boldsymbol{\tau}}_b^b = \begin{bmatrix}\bar{\tau}_\phi & \bar{\tau}_\theta & \bar{\tau}_\Psi\end{bmatrix}^{\mathrm{T}}$ a new virtual control input after the feedback linearization. Folding it in (27b) and considering (24) transform the dynamic model (27) in the following extended form

$$m\ddot{x} = -u(c_\phi s_\theta c_\Psi + s_\phi s_\Psi), \tag{28a}$$
$$m\ddot{y} = -u(c_\phi s_\theta s_\Psi - s_\phi c_\Psi), \tag{28b}$$
$$m\ddot{z} = mg - uc_\phi c_\theta, \tag{28c}$$
$$\ddot{\phi} = \bar{\tau}_\phi, \tag{28d}$$
$$\ddot{\theta} = \bar{\tau}_\theta, \tag{28e}$$
$$\ddot{\Psi} = \bar{\tau}_\Psi. \tag{28f}$$

IV. Orbital stabilization

The objective is now to apply the orbital stabilization tools revised in Section II to the dynamic model of a VToL UAV (28). However, notice that $n = 6$ and $m = 4$ in (28), while only the case $n - m = 1$ is allowed from the theory. Therefore, one component of (28) has to be dropped. Since the flat outputs of (28) are the x, y, z, Ψ components [18], and since for landing purposes the z component is absolutely necessary, then the made choice is to drop the y component, without loss of generality. The dynamic equation (28b) is thus ignored only for control purposes. After these considerations, comparing (1) and (28) yields

$$\boldsymbol{B}(\boldsymbol{q}) = \mathrm{diag}(\begin{bmatrix} m & m & 1 & 1 & 1 \end{bmatrix}), \tag{29a}$$
$$\boldsymbol{C}(\boldsymbol{q}, \dot{\boldsymbol{q}}) = \boldsymbol{O}_5, \tag{29b}$$
$$\boldsymbol{g}(\boldsymbol{q}) = \begin{bmatrix} 0 & -mg & 0 & 0 & 0 \end{bmatrix}^{\mathrm{T}}, \tag{29c}$$
$$\boldsymbol{G}(\boldsymbol{q}) = \begin{bmatrix} -c_\phi s_\theta c_\Psi - s_\phi s_\Psi & 0 & 0 & 0 \\ -c_\phi c_\theta & 0 & 0 & 0 \\ 0 & 1 & 0 & 0 \\ 0 & 0 & 1 & 0 \\ 0 & 0 & 0 & 1 \end{bmatrix}, \tag{29d}$$

with $\boldsymbol{q} = \begin{bmatrix} x & z & \phi & \theta & \Psi \end{bmatrix}^{\mathrm{T}}$ and $\boldsymbol{\tau} = \begin{bmatrix} u & \bar{\tau}_\phi & \bar{\tau}_\theta & \bar{\tau}_\Psi \end{bmatrix}^{\mathrm{T}}$.

The choice of the virtual geometric constraints (2) is the key of the constructive method: it offers a way to restraint the system coordinates to follow some virtual imposed path and obtain a virtual limit system with a periodic solution to track. In turn, the choice of λ is then essential. This can be chosen as a single coordinate of $\boldsymbol{q}$ or as a combination of q_i. Since λ is the parameter of the limit cycle (3), which is also the periodic trajectory of the landing platform, then it is worth to choose such a parameter as either the coordinate x or the coordinate z of the aerial vehicle. In the former case, it is possible to have a longitudinal oscillation of the landing platform (i.e., an oscillating sliding track); in the latter case, it is instead possible to have a vertical oscillation of the landing platform (i.e, a ship's deck on a rough sea). Without loss of generality, the former case is considered from now on. Therefore, in general, the following set of constraints can be imposed

$$x = \lambda, \tag{30a}$$
$$z = f_z(\lambda), \tag{30b}$$
$$\phi = f_\phi(\lambda), \tag{30c}$$
$$\theta = f_\theta(\lambda), \tag{30d}$$
$$\Psi = f_\Psi(\lambda), \tag{30e}$$

with $f_z, f_\phi, f_\theta, f_\Psi$ some general scalar smooth functions in the argument λ. Hence, the terms in (5) become

$$\alpha(\lambda) = m - m f_z' \left(\sec f_\theta \sin f_\Psi \tan f_\phi + \cos f_\Psi \tan f_\theta\right), \tag{31a}$$
$$\beta(\lambda) = -m f_z'' \sec f_\theta \left(\cos f_\Psi \sin f_\theta + \sin f_\Psi \tan f_\phi\right), \tag{31b}$$
$$\gamma(\lambda) = mg \sec f_\theta \left(\cos f_\Psi \sin f_\theta + \sin f_\Psi \tan f_\phi\right). \tag{31c}$$

In order to obtain regular virtual constraints, the following conditions have to be matched: $\alpha(\lambda) \neq 0$, $\gamma(\lambda) \neq 0$ at least in an isolated point, $\cos f_\theta \neq 0$, $\cos f_\phi \neq 0$. Therefore, the virtual holonomic constraints chosen in this paper are

$$x = \lambda, \tag{32a}$$
$$z = z^\star, \tag{32b}$$
$$\phi = \mathrm{atan}(\nu\lambda), \tag{32c}$$
$$\theta = 0, \tag{32d}$$
$$\Psi = \frac{\pi}{2}, \tag{32e}$$

where $z^\star \in \mathbb{R}$ is a constant reference for the altitude, while $\nu > 0$ is a parameter to be tuned. The relations in (32) yield $\alpha = m$, $\beta = 0$, $\gamma = mg\nu\lambda$ and the following virtual limit system

$$\ddot{\lambda} + g\nu\lambda = 0, \tag{33}$$

which exhibits the following periodic solution if $\nu > 0$

$$\lambda^\star(t) = A_\lambda \sin\left(\frac{2\pi}{T} t + \vartheta_\lambda\right), \tag{34}$$

with $T = \frac{2\pi}{\sqrt{g\nu}}$.

The coordinates (9) are then defined as $y_1 = z - z^\star$, $y_2 = \phi - \mathrm{atan}(\nu\lambda)$, $y_3 = \theta$, $y_4 = \Psi - \frac{\pi}{2}$. Hence, the terms in (12) and (13) assume the following form

$$\boldsymbol{L}(\boldsymbol{\varsigma}) = \begin{bmatrix} 0 & 0 & 0 & 0 & 1 \\ 1 & 0 & 0 & 0 & 0 \\ 0 & 1 & 0 & 0 & \frac{\nu}{1+\nu^2\lambda^2} \\ 0 & 0 & 1 & 0 & 0 \\ 0 & 0 & 0 & 1 & 0 \end{bmatrix}, \tag{35a}$$
$$\boldsymbol{n}(\boldsymbol{\varsigma}, \dot{\boldsymbol{\varsigma}}) = \begin{bmatrix} 0 & 0 & -2\frac{\nu^3\dot{\lambda}^2\lambda}{(1+\nu^2\lambda^2)^2} & 0 & 0 \end{bmatrix}^{\mathrm{T}}, \tag{35b}$$
$$\boldsymbol{K}(\boldsymbol{\varsigma}) = \begin{bmatrix} -\frac{c_\phi c_\theta}{m} & 0 & 0 & 0 \\ \frac{\nu(s_\phi s_\Psi + c_\phi c_\Psi s_\theta)}{m+\nu^2\lambda^2} & 1 & 0 & 0 \\ 0 & 0 & 1 & 0 \\ 0 & 0 & 0 & 1 \end{bmatrix}, \tag{35c}$$
$$\boldsymbol{w}(\boldsymbol{\varsigma}, \dot{\boldsymbol{\varsigma}}) = \begin{bmatrix} g & 2\frac{\nu^3\dot{\lambda}^2\lambda}{1+\nu^2\lambda^2} & 0 & 0 \end{bmatrix}^{\mathrm{T}}. \tag{35d}$$

Notice that the matrices $\boldsymbol{L}(\boldsymbol{\varsigma})$ in (35a) and $\boldsymbol{K}(\boldsymbol{\varsigma})$ in (35c) are invertible in all the state space. Therefore, the feedback linearization (14) brings the system as in (15).

In the considered case, the terms in (16a) are represented by the following expressions

$$\boldsymbol{g}_y^\star = \begin{bmatrix} 0 & -\frac{mg}{2}\sec^2(\mathrm{atan}(\nu\lambda)) & 0 & 0 \end{bmatrix}^{\mathrm{T}}, \tag{36a}$$
$$\boldsymbol{g}_{\dot{y}}^\star = \boldsymbol{0}_4, \tag{36b}$$
$$\boldsymbol{g}_v^\star = \begin{bmatrix} m\nu\lambda & 0 & 0 & 0 \end{bmatrix}^{\mathrm{T}}. \tag{36c}$$

The terms (19), belonging to the matrices $\boldsymbol{A}(t)$ and $\boldsymbol{V}(t)$ in (17), become instead

$$\kappa_1(t) = 0, \tag{37a}$$
$$\boldsymbol{\kappa}_2(t) = \begin{bmatrix} 0 & -g\dot{\lambda}^\star(t)\sec^2(\mathrm{atan}(\nu\lambda^\star(t))) & 0 & 0 \end{bmatrix}^{\mathrm{T}}, \tag{37b}$$
$$\boldsymbol{\kappa}_3(t) = \boldsymbol{0}_4, \tag{37c}$$
$$\boldsymbol{\rho}(t) = \begin{bmatrix} 2\nu\dot{\lambda}^\star(t)\lambda^\star(t) & 0 & 0 & 0 \end{bmatrix}^{\mathrm{T}}. \tag{37d}$$

The controllability of the resulting $\boldsymbol{A}(t)$ and $\boldsymbol{V}(t)$ matrices is given in Appendix B. Finally, the integral of motion is

$$I(\lambda, \dot{\lambda}, \lambda^\star(0), \dot{\lambda}^\star(0)) = \dot{\lambda}^2 - \dot{\lambda}^{\star^2}(0) + g\nu(\lambda^2 - \lambda^{\star^2}(0)). \tag{38}$$

With the above matrices and vectors, by applying (14) and (22) to (28) it is possible to asymptotically constraint the aerial vehicle to relations (32) while following the periodic orbit (34). Nevertheless, notice that the z component in (32b) has been chosen to be constant. In order to land on the oscillating platform, this reference has to change during the task. Therefore, the strategy plan is to give a slow-varying reference to z once the orbital trajectory has been stabilized. Notice that a similar philosophy can be found in [10]. No theoretical proof is given to ensure asymptotic stability with a time varying constraint in (32b). However, performances of the resulting control strategy are provided in the next section.

V. Case studies

The presented approach is now validated through dynamic simulations in the MATLAB/SIMULINK environment. With reference to Fig. 1, a quadrotor is considered as the chosen VToL UAV. The aerial vehicle has mass $m = 1.25$ kg and inertia $\boldsymbol{J}_b = \text{diag}(\begin{bmatrix}1.25 & 1.25 & 2.5\end{bmatrix})$ m^2 kg.

In order to investigate the landing of an aerial vehicle on a platform longitudinally oscillating (i.e., a sliding track or a ship's deck in some particular conditions of the sea), the following scenario is taken into account. Consider a rover equipped with a robotic arm. A plate on which the quadrotor has to land is attached at the robot's end-effector. The rover performs an oscillating trajectory. Its motion is planned through a closed-loop inverse kinematics algorithm [19]. Such envisioned case study might reproduces the same effects of real scenarios, and it could also be easily reproduced in research labs. The periodic movement has the following parameters: $A_\lambda = 0.5$ m, $T = 5$ s and $\vartheta_\lambda = \frac{\pi}{4}$ rad. From the period T, it is possible to retrieve the value of ν that is equal to 0.161. As for other applications, notice that such values could also represent the results of a proper module estimating the periodic motion of the oscillating landing platform.

The chosen initial conditions for the UAV are $x(0) = 0.46$ m, $y(0) = 0$ m, $z(0) = -2$ m, $\phi(0) = \theta(0) = 0$, $\Psi(0) = \frac{\pi}{2}$ rad, $\dot{x}(0) = 0.31$ m/s, $\dot{y}(0) = \dot{z}(0) = 0$ m/s and $\dot{\phi}(0) = \dot{\theta}(0) = \dot{\Psi}(0) = 0$ rad/s. Notice that the initial conditions for the x component are different from the desired ones achievable from (34): $x^\star(0) = \lambda^\star(0) = A_\lambda \sin(\vartheta_\lambda) = 0.35$ m and $\dot{x}^\star(0) = \dot{\lambda}^\star(0) = \frac{2\pi A_\lambda}{T}\cos(\vartheta_\lambda) = 0.44$ m/s. The periodic Riccati equation (21) has been solved through the convex optimization solver proposed in [20]. The gains have been experimentally tuned as $\boldsymbol{\Gamma} = 0.1\boldsymbol{I}_4$ and $\boldsymbol{\Theta} = \text{diag}(\begin{bmatrix}10 & 600 & 100 & 100 & 100 & 2000 & 1 & 1 & 10\end{bmatrix})$.

For each case study, the entire task lasts 60 s. The trajectory for the z component is planned as follows: for the first 5 s, z is kept at its initial value $z(0) = -2$ m, while it reaches the landing altitude of -0.75 m with a linear path at 45 s. Until the end of the task, the reference is then kept at -0.75 m, which is also the altitude with respect to Σ_i of the plate mounted on the mobile manipulator.

A first case study is performed to verify the performances of the proposed method in ideal conditions. A video of this first simulation is present as multimedia attachment to this manuscript. The plots in Fig. 2 show how the quadrotor is able to recover from its initial configuration, track the periodic motion of the oscillating platform and safely land on it. In particular, the altitude error is represented in Fig. 2(a). It is possible to notice that when the altitude reference is kept constant (i.e., before 5 s and after 45 s) the closed-loop system asymptotically reaches the desired value. On the other hand, a constant error is exhibited by the system when z is a function of time. Notice that the virtual constraints in (2) have to be only geometric and not time dependent, like instead considered for the altitude. Since the planner for the z component is a ramp between 5 s and 45 s, the system acts like an integrator making the tracking error a constant.

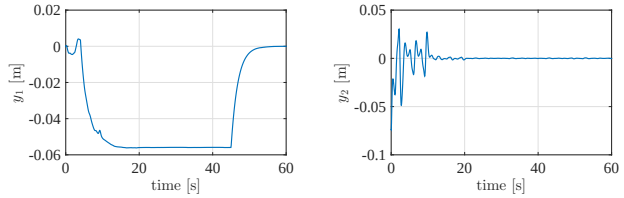

(a) Time history of $y_1 = z - z^\star(t)$ for the first case study.

(b) Time history of $y_2 = \phi - \text{atan}(\nu\lambda)$ for the first case study.

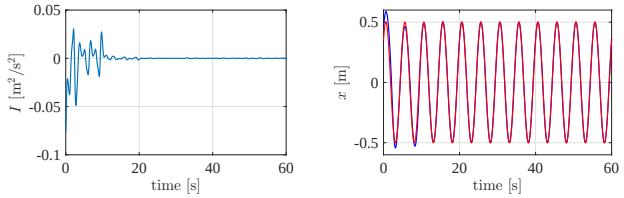

(c) Time history of the integral of motion I for the first case study.

(d) Comparison between the time history of x, in blue, and the reference motion for the landing platform $\lambda^\star(t)$, in red, for the first case study.

Fig. 2. Time histories for the first case study.

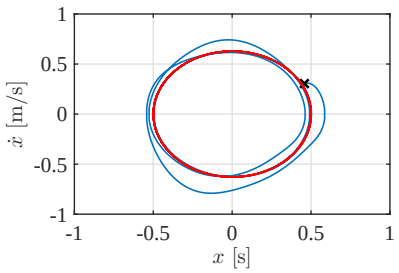

Fig. 3. Phase portrait relative to the first case study. In red the orbit generated by $(\lambda^\star(t), \dot{\lambda}^\star(t))$. In blue the phase portrait generated by $(x(t), \dot{x}(t))$. The black cross represents the starting point $(x(0), \dot{x}(0))$.

This constant error depends on both the initial conditions of the UAV and the gains chosen to solve the periodic Riccati equation. The error related to the roll angle ϕ is instead depicted in Fig. 2(b) and it asymptotically converges to zero. The integral of motion preserves its zero value along the desired trajectory $\lambda^\star(t)$ as illustrated in Fig. 2(c). The time history for y_3 and y_4 have been neglected since they present very small values for all the task and do not exhibit any relevant information. On the other hand, from Fig. 2(d), it is possible to appreciate how the x component of the quadrotor is able to follow the desired periodic trajectory (34). Finally, the phase portrait in Fig. 3 shows in a intuitive way the stabilization of the desired orbital trajectory (in red in the figure). Starting from a condition which is not on the desired orbit (black cross in the figure), the developed controller is able to bring back the UAV on the desired periodic motion.

A second case study is also performed to test the developed controller in presence of Gaussian white noise (GWN) on the measurements. In particular, the UAV usually suffers from corrupted measures given by the on-board IMU and the estimation module giving the information about

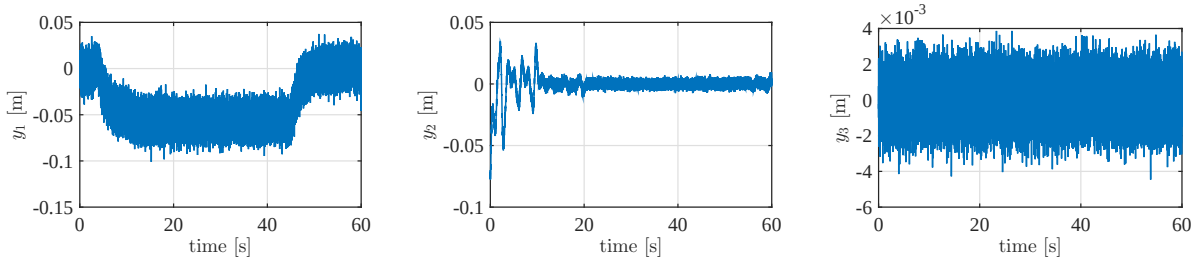

(a) Time history of $y_1 = z - z^\star(t)$ for the second case study.

(b) Time history of $y_2 = \phi - \text{atan}(\nu\lambda)$ for the second case study.

(c) Time history of $y_3 = \theta$ for the second case study.

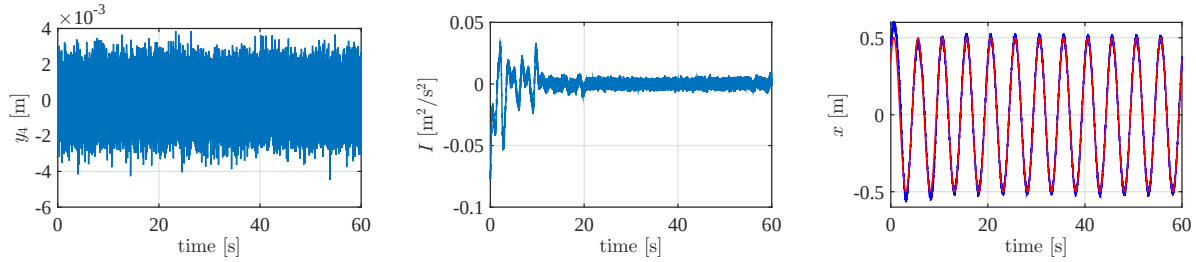

(d) Time history of $y_4 = \Psi - \frac{\pi}{2}$ for the second case study.

(e) Time history of the integral of motion I for the second case study.

(f) Comparison between the time history of x, in blue, and the reference motion for the landing platform $\lambda^\star(t)$, in red, for the second case study.

Fig. 4. Time histories for the second case study.

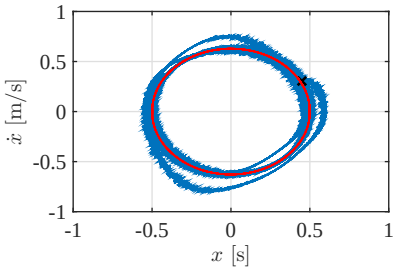

Fig. 5. Phase portrait relative to the second case study. In red the orbit generated by $(\lambda^\star(t), \dot{\lambda}^\star(t))$. In blue the phase portrait generated by $(x(t), \dot{x}(t))$. The black cross represents the starting point $(x(0), \dot{x}(0))$.

the absolute position of the aerial vehicle (e.g., a Kamlan filter combining GPS, optical flow, accelerometers and other measurements) [21]. For the translational part, a GWN with standard deviation equals to 10^{-2} is assumed. For the rotational part, a GWN with standard deviation equals to 10^{-3} is instead considered. These values are reliable for commercial sensors and standard outdoor aerial applications. The performances of the controller are shown in Fig. 4. The same comments given for the first case study hold. The time histories relative to y_2 and y_3 are shown in Fig. 4(c) and Fig. 4(d), respectively. The phase portrait for this second example is depicted in Fig. 5. The developed controller is thus robust with respect to measurements affected by GWN.

VI. Conclusion and Future Work

An orbital stabilization for safe landing of a VToL UAV is presented in this paper. A set of virtual holonomic constraints is introduced, pushing the system to reach a limit cycle corresponding to the desired periodic trajectory. Simulative case studies bolster the performances of the proposed approach.

This preliminary work is necessary to develop a sequence of improvements, some of them are already under development. First, it is not desirable to neglect one horizontal translational coordinate of the VToL UAV. This choice has been made because of the request to have a degree of underactuation equals to one. The general approach proposed in [22] may help about this aspect. Moreover, the desired periodic trajectory should not be simply a sine term with a given amplitude, frequency and phase. Looking at the cited works in the introduction, a finite (or infinite) sum of sine and cosine terms is often employed to describe the movement of an oscillating platform. In the proposed approach, instead, the periodic solution is a result of the virtual limit system (3) guided by the selected virtual holonomic constraints (2). Giving the desired oscillating trajectory and obtaining in turn the constraints is a future development. Last, but not least, it is very challenging to check how the proposed approach deals with the case of a changing behaviour of the oscillating platform. For instance, it might be interesting to see both the introduction of time-varying virtual constraints in (2) and how to cope with the problem of having A_λ, T, and ϑ_λ as function of time.

Appendix A

In order to obtain the expression (15a), the following scalar equation has to be considered

$$\boldsymbol{\iota}(\boldsymbol{q})^{\mathrm{T}} \left(\boldsymbol{B}(\boldsymbol{q}) \left(\boldsymbol{L}(\boldsymbol{\varsigma})\ddot{\boldsymbol{\varsigma}} + \boldsymbol{n}(\boldsymbol{\varsigma}, \dot{\boldsymbol{\varsigma}}) \right) + \boldsymbol{C}(\boldsymbol{q}, \dot{\boldsymbol{q}})\dot{\boldsymbol{q}} + \boldsymbol{g}(\boldsymbol{q}) \right) = 0, \tag{39}$$

with $q_1 = y_1 + \phi_1(\lambda), \ \ldots, q_{n-1} = y_{n-1} + \phi_{n-1}(\lambda)$, $q_n = \phi_n(\lambda) + h(\boldsymbol{\varsigma})$ and $\dot{\boldsymbol{q}} = \boldsymbol{L}(\boldsymbol{\varsigma})\dot{\boldsymbol{\varsigma}}$. Developing computations yields

$$\alpha(\lambda)\ddot{\lambda} + \beta(\lambda)\dot{\lambda}^2 + \gamma(\lambda) = f(\boldsymbol{a}, \boldsymbol{b}), \tag{40}$$

with $\boldsymbol{a} = \begin{bmatrix}\boldsymbol{y}^{\mathrm{T}} & \dot{\boldsymbol{y}}^{\mathrm{T}} & \boldsymbol{\upsilon}^{\mathrm{T}}\end{bmatrix}^{\mathrm{T}} \in \mathbb{R}^{3m}$ and $\boldsymbol{b} = \begin{bmatrix}\lambda & \dot{\lambda} & \ddot{\lambda}\end{bmatrix}^{\mathrm{T}} \in \mathbb{R}^3$. Using the first-order form of the Taylor's theorem, it is possible to write

$$\begin{aligned} f(\boldsymbol{a}, \boldsymbol{b}) = f(\boldsymbol{0}_{3m}, \boldsymbol{b}) &+ \boldsymbol{y}^{\mathrm{T}} \int_0^1 \left(\frac{\partial f(\sigma \boldsymbol{a}, \boldsymbol{b})}{\partial \boldsymbol{y}}\right)^{\mathrm{T}} \mathrm{d}\sigma \\ &+ \dot{\boldsymbol{y}}^{\mathrm{T}} \int_0^1 \left(\frac{\partial f(\sigma \boldsymbol{a}, \boldsymbol{b})}{\partial \dot{\boldsymbol{y}}}\right)^{\mathrm{T}} \mathrm{d}\sigma \\ &+ \boldsymbol{\upsilon}^{\mathrm{T}} \int_0^1 \left(\frac{\partial f(\sigma \boldsymbol{a}, \boldsymbol{b})}{\partial \boldsymbol{\upsilon}}\right)^{\mathrm{T}} \mathrm{d}\sigma. \end{aligned} \tag{41}$$

From (41) it is straightforward to show how (40) can be brought as (15a).

APPENDIX B

From classical control theory, it is well-known that a linear periodic system (17) is controllable over the period T if and only if the following Grammian matrix

$$\boldsymbol{Z} = \int_0^T \boldsymbol{X}(t)^{-1} \boldsymbol{V}(t)^{\mathrm{T}} \boldsymbol{V}(t) (\boldsymbol{X}(t)^{\mathrm{T}})^{-1} \mathrm{d}t \in \mathbb{R}^{2m+1 \times 2m+1} \tag{42}$$

is positive definite, where the matrix $\boldsymbol{X}(t) \in \mathbb{R}^{2m+1 \times 2m+1}$ is the solution of the following differential equation

$$\dot{\boldsymbol{X}}(t) = \boldsymbol{A}(t)\boldsymbol{X}(t), \tag{43}$$

with $\boldsymbol{X}(0) = \boldsymbol{I}_{2m+1}$.

Considering the expressions of $\boldsymbol{A}(t)$ and $\boldsymbol{V}(t)$ in (18a) and (18b), respectively, with the related terms in (37), the matrix $\boldsymbol{X}(t)$ can be verified to have the following expression

$$\boldsymbol{X}(t) = \begin{bmatrix} 1 & e^{\int_0^t \boldsymbol{\kappa}_2(s)^{\mathrm{T}} \mathrm{d}s} & \boldsymbol{0}_4^{\mathrm{T}} \\ \boldsymbol{0}_4 & \boldsymbol{I}_4 & t\boldsymbol{I}_4 \\ \boldsymbol{0}_4 & \boldsymbol{O}_4 & \boldsymbol{I}_4 \end{bmatrix}, \tag{44}$$

with $\boldsymbol{\kappa}_2(t)$ as in (37b). For each of the case studies in Section V, the matrix $\boldsymbol{Z}$ in (42) has been numerically verified to be positive definite. As a matter of fact, the resulting matrices are symmetric with all positive eigenvalues.

REFERENCES

[1] F. Ruggiero, M. Trujillo, R. Cano, H. Ascorbe, A. Viguria, C. Peréz, V. Lippiello, A. Ollero, and B. Siciliano, "A multilayer control for multirotor UAVs equipped with a servo robot arm," in *2015 IEEE International Conference on Robotics and Automation*, Seattle, WA, USA, 2015, pp. 4014–4020.

[2] F. Ruggiero, J. Cacace, H. Sadeghian, and V. Lippiello, "Impedance control of VToL UAVs with a momentum-based external generalized forces estimator," in *2014 IEEE International Conference on Robotics and Automation*, Hong Kong, C, 2014, pp. 2093–2099.

[3] F. Ruggiero, J. Cacace, H. Sadeghian, and V. Lippiello, "Passivity-based control of VToL UAVs with a momentum-based estimator of external wrench and unmodeled dynamics," *Robotics and Autonomous Systems*, vol. 72, pp. 139–151, 2015.

[4] V. Lippiello, F. Ruggiero, and D. Serra, "Emergency landing for a quadrotor in case of a propeller falure: A PID based approach," in *IEEE 12th International Symposium on Safety, Security and Rescue Robotics*, Toyako-Cho, J, 2014.

[5] V. Lippiello, F. Ruggiero, and D. Serra, "Emergency landing for a quadrotor in case of a propeller failure: A backstepping approach," in *2014 IEEE/RSJ International Conference on Intelligent Robots and Systems*, Chicago, IL, USA, 2014, pp. 4782–4788.

[6] J. R. Hervas, M. Reyhanoglu, and H. Tang, "Automatic landing control of unmanned aerial vehicles on moving platforms," in *2014 IEEE 23rd International Symposium on Industrial Electronics*, Instanbul, T, 2014, pp. 69–74.

[7] J. Sanchez-Lopez, J. Pestana, S. Saripalli, and P. Campoy, "An approach toward visual autonomous ship board landing of a VTOL UAV," *Journal of Intelligent Robots and Systems*, vol. 74, pp. 113–127, 2014.

[8] S. Lin, M. Garratt, A. Lambert, and P. Li, "6DoF estimation for UAV landing on a moving shipdeck using real-time on-board vision," in *Australian Control Conference on Robotics and Automation*, Canberra, AUS, 2015.

[9] L. Marconi, A. Isidori, and A. Serrani, "Autonomous vertical landing on an oscillating platform: an internal-model based approach," *Automatica*, vol. 38, pp. 21–32, 2002.

[10] B. Hérissé, T. Hamel, R. Mahony, and F.-X. Russotto, "Landing a VTOL unmanned aerial vehicle on a moving platform using optical flow," *IEEE Transactions on Robotics*, vol. 28, no. 1, pp. 77–89, 2012.

[11] B. Hu, L. Lu, and S. Mishra, "Fast, safe and precise landing of a quadrotor on an oscillating platform," in *2015 American Control Conference*, Chicago, IL, USA, 2015, pp. 3836–3841.

[12] A. S. Shiriaev, J. Perram, and C. Canudas-de Wit, "Constructive tool for orbital stabilization of underactuated nonlinear systems: Virtual constraints approach," *IEEE Transactions on Automatic Control*, vol. 50, no. 8, pp. 1164–1176, 2005.

[13] M. Surov, A. Shiriaev, L. Freidovich, S. Gusev, and L. Paramonov, "Case study in non-prehensile manipulation: Planning perpetual rotations for "Butterfly" robot," in *2015 IEEE International Conference on Robotics and Automation*, Seattle, WA, USA, 2015, pp. 1484—1489.

[14] S. Westerberg, U. Mettin, A. S. Shiriaev, L. B. Freidovich, and Y. Orlov, "Motion planning and control of a simplified helicopter model based on virtual holonomic constraints," in *2009 International Conference on Advanced Robotics*, Munich, D, 2009, pp. 1–6.

[15] S. Westerberg, U. Mettin, and A. S. Shiriaev, "Motion planning and control of an underactuated 3DOF helicopter," in *2010 IEEE/RSJ International Conference on Intelligent Robots and Systems*, Taipei, ROC, 2010, pp. 3759–3764.

[16] M. Maggiore and L. Consolini, "Virtual holonomic constraints for Euler-Lagrange systems," *IEEE Transactions on Automatic Control*, vol. 58, no. 4, pp. 1001–1008, 2013.

[17] K. Nonami, F. Kendoul, S. Suzuki, and W. Wang, *Autonomous Flying Robots. Unmanned Aerial Vehicles and Micro Aerial Vehicles*. Berlin Heidelberg, D: Springer-Verlag, 2010.

[18] P. Fliess, J. Levine, and P. Rouchon, "Flatness and defect of nonlinear systems: Introductory theory and examples," *International Journal of Control*, vol. 61, no. 6, pp. 1327–1361, 1995.

[19] B. Siciliano, L. Sciavicco, L. Villani, and G. Oriolo, *Robotics: Modelling, Planning and Control*. London, UK: Springer, 2008.

[20] S. Gusev, S. Johansson, B. Kagstrom, A. Shiriaev, and A. Varga, "A numerical evaluation of solvers for the periodic Riccati differential equation," *BIT Numerical Mathematics*, vol. 50, no. 2, pp. 301–329, 2010.

[21] V. Lippiello and R. Mebarki, "Closed-form solution for absolute scale velocity estimation using visual and inertial data with a sliding least-squares estimation," in *21st Mediterranean Conference on Control and Automation*, Crete, G, 2013.

[22] A. S. Shiriaev, L. B. Freidovich, and S. V. Gusev, "Transverse linearization for controlled mechanical systems with several passive degrees of freedom," *IEEE Transactions on Automatic Control*, vol. 55, no. 4, pp. 893–906, 2010.